References and Notes

1. M. A. Richards, R. A. Duncan, V. E. Courtillot, *Science* **246**, 103 (1989).
2. V. E. Courtillot, P. R. Renne, *C. R. Geosci.* **335**, 113 (2003).
3. R. E. Ernst, K. L. Buchan, *Geol. Soc. Am. Spec. Pap.* **352**, 483 (2001).
4. M. W. McElhinny, N. D. Opdyke, *J. Geophys. Res.* **69**, 2465 (1964).
5. H. L. Allsopp, J. D. Kramers, D. L. Jones, A. J. Erlank, *S. Afr. J. Geol.* **92**, 11 (1989).
6. R. E. Hanson, M. W. Martin, S. A. Bowring, H. Munyanyiwa, *Geology* **26**, 1143 (1998).
7. H. Munyanyiwa, *J. Afr. Earth Sci.* **28**, 349 (1999).
8. P. B. Groenewald, A. B. Moyes, G. H. Grantham, J. R. Krynauw, *Precambrian Res.* **75**, 231 (1995).
9. M. W. McElhinny, *Geophys. J. R. Astron. Soc.* **10**, 375 (1966).
10. A. B. Kampunzu, P. Akanyang, R. B. M. Mapeo, B. N. Modie, M. Wendorff, *Geol. Mag.* **135**, 669 (1998).
11. S. E. Ward, R. P. Hall, D. J. Hughes, *J. Afr. Earth Sci.* **30**, 689 (2000).
12. Materials and methods are available as supporting material on *Science* Online.
13. Age uncertainties are stated at the 2σ level. For sample 96-141 (*12*) in eastern Zimbabwe, Hanson *et al.* (*6*) reported U-Pb zircon isotopic analyses that were 1.9 to 17.9% discordant. They inferred that the $^{207}Pb/^{206}Pb$ date for the most concordant grain (1104.7 ± 2.3 Ma) provided the best estimate of the age of the sill. This result is superseded by new analyses reported in fig. S4 and table S2, which yield a weighted mean $^{207}Pb/^{206}Pb$ date of 1109.6 ± 0.6 Ma (Fig. 1).
14. D. W. Davis, J. C. Green, *Can. J. Earth Sci.* **34**, 476 (1997).
15. D. J. Allen, W. J. Hinze, A. B. Dickas, M. G. Mudrey Jr., *Geol. Soc. Am. Spec. Pap.* **312**, 47 (1997).
16. H. C. Halls, L. J. Pesonen, *Geol. Soc. Am. Mem.* **156**, 173 (1982).
17. J. E. French, L. M. Heaman, T. Chacko, *Chem. Geol.* **188**, 85 (2002).
18. L. L. Shastri, K. R. Chamberlain, S. A. Bowring, *Geol. Soc. Am. Abstr. Program* **23**, 93 (1991).
19. L. M. Heaman, J. P. Grotzinger, *Geology* **20**, 637 (1992).
20. S. A. Bowring, unpublished data.
21. S. S. Harlan, *Can. J. Earth Sci.* **30**, 1415 (1993).
22. A. B. Weil, J. W. Geissman, M. Heizler, R. Van der Voo, *Tectonophysics* **375**, 199 (2003).
23. P. F. Hoffman, *Science* **252**, 1409 (1991).
24. S. A. Pisarevsky, M. T. D. Wingate, C. McA. Powell, S. Johnson, D. A. D. Evans, *Geol. Soc. London Spec. Pub.* **206**, 35 (2003).
25. K. L. Buchan *et al.*, *Precambrian Res.* **110**, 9 (2001).
26. J. G. Meert, T. H. Torsvik, *Tectonophysics* **375**, 261 (2003).
27. I. W. D. Dalziel, S. Mosher, L. M. Gahagan, *J. Geol.* **108**, 499 (2000).
28. In the absence of an independent polarity constraint, the near-zero inclination of the Umkondo magnetization direction, resulting from the equatorial position of Kalahari ~1100 Ma, permits either polarity assignment and makes it possible to rotate Kalahari by 180° without shifting its latitudinal position.
29. I. W. D. Dalziel, L. A. Lawver, J. B. Murphy, *Earth Planet. Sci. Lett.* **178**, 1 (2000).
30. M. T. D. Wingate, F. Pirajno, P. A. Morris, *Geology* **32**, 105 (2004).
31. M. Gurnis, *Nature* **332**, 695 (1988).
32. L. Guillou, C. Jaupart, *J. Geophys. Res.* **100**, 24217 (1995).
33. D. L. Anderson, *Geology* **22**, 39 (1994).
34. D. L. Anderson, *Science* **293**, 2016 (2001).
35. S. D. King, D. L. Anderson, *Earth Planet. Sci. Lett.* **160**, 289 (1998).
36. L. M. Heaman, N. Machado, *Contrib. Mineral. Petrol.* **110**, 289 (1992).
37. R. E. Zartman, S. W. Nicholson, W. F. Cannon, G. B. Morey, *Can. J. Earth Sci.* **34**, 549 (1997).
38. C. V. Reeves, B. K. Sahu, M. de Wit, *J. Afr. Earth Sci.* **34**, 101 (2002).
39. R. E. Hanson, *Geol. Soc. London Spec. Pub.* **206**, 427 (2003).
40. W. Bauer, R. J. Thomas, J. Jacobs, *Geol. Soc. London Spec. Pub.* **206**, 247 (2003).
41. S. J. Singletary *et al.*, *Precambrian Res.* **121**, 47 (2003).
42. A. B. Kampunzu, R. A. Armstrong, M. P. Modisi, R. B. M. Mapeo, *J. Afr. Earth Sci.* **30**, 579 (2000).
43. M. O. Schwartz, Y. Y. Kwok, D. W. Davis, P. Akanyang, *S. Afr. J. Geol.* **99**, 245 (1996).
44. N. Pfurr, H. Ahrendt, B. T. Hansen, K. Weber, *Communs. Geol. Surv. Namibia* **7**, 35 (1991).
45. M. T. D. Wingate, *S. Afr. J. Geol.* **104**, 13 (2001).
46. W. R. Van Schmus, M. W. Martin, D. R. Sprowl, J. Geissman, P. Berendsen, *Geol. Soc. Am. Abstr. Program* **22**, A174 (1990).
47. For the Midcontinent rift, we used the average of the published poles for the Logan sills, Coldwell Complex, Powder Mill Group, and North Shore Volcanic Group (*16*, *21*), which have yielded U-Pb crystallization ages of 1107.9 ± 1.8 to 1108 ± 1 Ma (*14*, *36*, *37*). The position of this average pole is 49.1°N, 209.2°E, with a radius for the 95% circle of confidence of 7.7°. Aligning this pole and the mean Umkondo pole places the two cratons ~3000 km apart. The separation could be decreased by ~1700 km if the extreme limits of the error circles for the poles were used.
48. G. R. Keller, J. M. Hills, M. R. Baker, E. T. Wallin, *Geology* **17**, 1049 (1989).
49. J. F. Wilson, D. L. Jones, J. D. Kramers, *Geol. Assoc. Can. Spec. Pap.* **34**, 433 (1987).
50. D. L. Jones, M. W. McElhinny, *J. Geophys. Res.* **71**, 543 (1966).
51. R. B. Hargraves, P. J. Hattingh, T. C. Onstott, *S. Afr. J. Geol.* **97**, 114 (1994).
52. M. Peters, *Ber. Polarforschung* **61**, 1 (1989).
53. D. L. Jones, M. P. Bates, Z. X. Li, B. Corner, G. Hodgkinson, *Tectonophysics* **375**, 247 (2003).

54. We thank G. Brandl for advice on sample sites in South Africa; T. Machacha (Director) and T. Majaule, Botswana Geological Survey, for permission to sample borehole cores from the Xade Complex; B. Vink and M. Wendorff for assistance in Botswana; F. Venter for permission to sample in Kruger National Park, South Africa, and J. Venter for assistance in the park; and A. Maloof for discussions of paleomagnetic data. Supported by NSF grant nos. EAR-9909269 (R.E.H.) and EAR-9909854 (I.W.D.D. and W.A.G.), and EAR-9526702 (S.A.B.), and by the Tectonics Special Research Centre, University of Western Australia (I.W.D.D.). This paper is dedicated to the memory of H. Munyanyiwa, who first pointed out to us the potential significance of the Umkondo sills in eastern Zimbabwe.

Supporting Online Material

www.sciencemag.org/cgi/content/full/1096329/DC1
Materials and Methods
SOM Text
Figs. S1 to S4
Tables S1 and S2
References and Notes

2 February 2004; accepted 1 April 2004
Published online 22 April 2004;
10.1126/science.1096329
Include this information when citing this paper.

REPORTS

Optical Signatures of the Aharonov-Bohm Phase in Single-Walled Carbon Nanotubes

Sasa Zaric,[1,4,5] Gordana N. Ostojic,[2,4,5] Junichiro Kono,[2,4,5]* Jonah Shaver,[1,4,5,6] Valerie C. Moore,[3,4,5,6] Michael S. Strano,[3,4,5,6]† Robert H. Hauge,[3,4,5,6] Richard E. Smalley,[1,3,4,5,6] Xing Wei[7]

We report interband magneto-optical spectra for single-walled carbon nanotubes in high magnetic fields up to 45 tesla, confirming theoretical predictions that the band structure of a single-walled carbon nanotube is dependent on the magnetic flux ϕ threading the tube. We have observed field-induced optical anisotropy as well as red shifts and splittings of absorption and photoluminescence peaks. The amounts of shifts and splittings depend on the value of ϕ/ϕ_0 and are quantitatively consistent with theories based on the Aharonov-Bohm effect. These results represent evidence of the influence of the Aharonov-Bohm phase on the band gap of a solid.

When a magnetic flux, ϕ, passes through a mesoscopic ring, the quantum states and dynamics of electrons on the ring are influenced by the Aharonov-Bohm (AB) phase (*1*); that is, $2\pi\phi/\phi_0$, where $\phi_0 = h/e$ is the magnetic flux quantum (h is the Planck constant and e is the electronic charge). When the phase coherence length exceeds the circumference, quantum interference between loop trajectories of opposite sense induces magnetoresistance oscillations with period ϕ_0 (known as AB oscillations) and $\phi_0/2$ [known as Altshuler-Aronov-Spivak (AAS) oscillations (*2*)]. These oscillations have been observed in various metallic rings and tubes (*3*), including the recent observation of the AAS oscillations in multiwalled carbon nanotubes (*4*).

[1]Department of Physics and Astronomy, [2]Department of Electrical and Computer Engineering, [3]Department of Chemistry, [4]Rice Quantum Institute, [5]Center for Nanoscale Science and Technology, [6]Center for Biological and Environmental Nanotechnology, Rice University, Houston, TX 77005 USA. [7]National High Magnetic Field Laboratory, Florida State University, Tallahassee, FL 32310, USA.

*To whom correspondence should be addressed. E-mail: kono@rice.edu.
†Present address: Department of Chemical and Biomolecular Engineering, University of Illinois, Urbana, IL 61801, USA.

Furthermore, a recent far-infrared study of semiconducting nanorings revealed AB phase–dependent spectral features (*5*).

A single-walled carbon nanotube (SWNT) is a tubular crystal of sp^2-bonded carbon atoms, whose basic properties (such as metallicity) are determined by a pair of integers, or chirality, (n,m). When threaded by ϕ, its band structure is predicted to depend on ϕ/ϕ_0 (*6*, *7*), a manifestation of the AB effect, having no counterpart in mesoscopic rings and arising from the fact that the periodic lattice potential along the circumferential direction strictly enforces the Bloch condition along exactly the paths that enclose the flux. Thus, in calculating the band structure, one has to take into account the interplay between the Bloch theorem and the AB effect. The circumferential boundary condition explicitly depends on ϕ/ϕ_0, and the band gap oscillates with period ϕ_0 (Fig. 1B). Consequences of these effects are expected to appear in various quantities (*6*–*13*), but most prominently in interband optical spectra as peak shifts and splittings (*7*, *12*, *13*). The splittings are due to degeneracy lifting [Ajiki-Ando (AA) splitting] (*6*, *7*), with the amount of splitting given by $\Delta E_{AA} \equiv 6E_g\phi/\phi_0$ when $\phi/\phi_0 < 1/6$ (Fig. 1, B and C). Recent success in preparing unbundled SWNTs in aqueous solutions led to the observation of chirality-dependent peaks in absorption and photoluminescence (PL) spectra (*14*) and to complete chirality assignments (*15*). This has opened ways to perform spectroscopy of SWNTs of specific chiralities.

We describe a magneto-optical study of SWNTs to directly verify these predictions. We measured absorption and PL in micelle-suspended SWNTs at magnetic fields (B) up to 45 T (*16*). In absorption, we observed splittings in some of the first-subband transition peaks (H_1 to E_1 in Fig. 1C), with the amount of splittings (30 to 40 meV at 45 T) consistent with the expected AA splitting. Splittings were not resolvable in the second-subband transitions (H_2 to E_2) because of their larger linewidths (~100 meV). Magneto-PL showed red shifts with increasing B for all observed peaks, the amount of which was diameter-dependent in a predicted way. Our detailed PL simulations, taking into account B-induced alignment of nanotubes, thermal population, and AA splittings, successfully reproduce the observed spectra, supporting our interpretation. It is important to point out that 45 T is not high enough to reveal a full period of the AB effect. For a typical nanotube diameter of 1 nm, 45 T corresponds to $\phi/\phi_0 = 8.55 \times 10^{-3}$.

Figure 2A shows polarization (P)–dependent magneto-absorption for the first-subband (E_1H_1) transitions measured in the Voigt geometry (with light propagation vector $\boldsymbol{k}$ perpendicular to the field). The solid and dashed lines are for parallel ($\boldsymbol{B}//\boldsymbol{P}$) and perpendicular ($\boldsymbol{B}\perp\boldsymbol{P}$) polarizations, respectively. The field induces changes in the spectrum. No traces are intentionally offset, so the P-dependent vertical shifts are real; that is, the B increases the absorption in the parallel case and decreases the absorption in the perpendicular case, resulting in large optical anisotropy. At 45 T, the absorption coefficient ratio ($\alpha_{//}/\alpha_{\perp}$) is ~4. The optical anisotropy, defined as $(\alpha_{//} - \alpha_{\perp})/(\alpha_{//} + \alpha_{\perp})$, is plotted versus energy for 0, 20, and 45 T (Fig. 2B), where the dotted lines are raw data and the solid lines are polynomial fits. At a given B, the anisotropy is larger for lower energies (corresponding to larger diameters). Because light polarized perpendicular to the tube axis is not absorbed (*7*), this indicates that larger-diameter tubes align better.

The field also induces spectral modifications. Each absorption peak broadens with increasing B, and finally some of the peaks split in the highest field range, 30 to 45 T only in the $\boldsymbol{B}//\boldsymbol{P}$ case (Fig. 2C). The typical linewidth of E_1H_1 transitions is ~20 meV, whereas the splitting is ~35 meV, indicating that the field range we used was just high enough. On the other hand, the typical linewidth of E_2H_2 transitions is large (~100 meV) because of the shorter carrier lifetimes and/or dephasing times in the second subbands (*17*). Therefore, as shown in Fig. 2D, B-induced spectral changes are not observable in the E_2H_2 transitions (the expected amount of splitting is the same as E_1H_1), although optical anisotropy is clearly present.

Figure 3A shows magneto-PL spectra up to 45 T, excited by a 633-nm He-Ne laser.

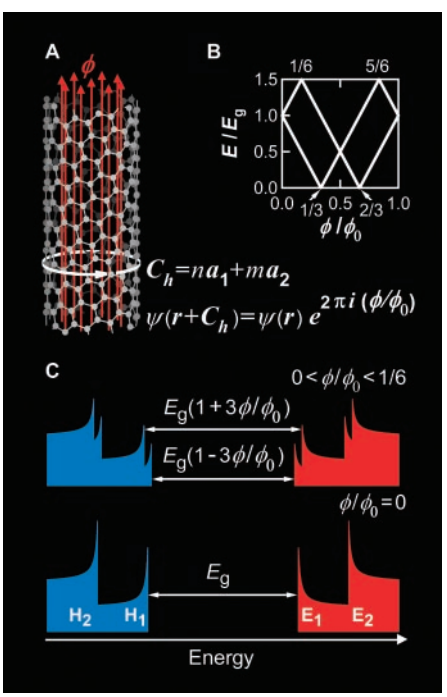

Fig. 1. (**A**) A SWNT with a chiral vector $\boldsymbol{C}_h$ = (10,3) threaded by a magnetic flux ϕ. (**B**) The predicted field dependence of the energy gap of a semiconducting nanotube (*7*). The two lines correspond to the K and K′ points in k space. (**C**) Schematic densities of states of the valence (blue) and conduction (red) bands of a semiconducting nanotube with (upper) and without (lower) a flux. The AB phase appears through the splitting of van Hove singularities.

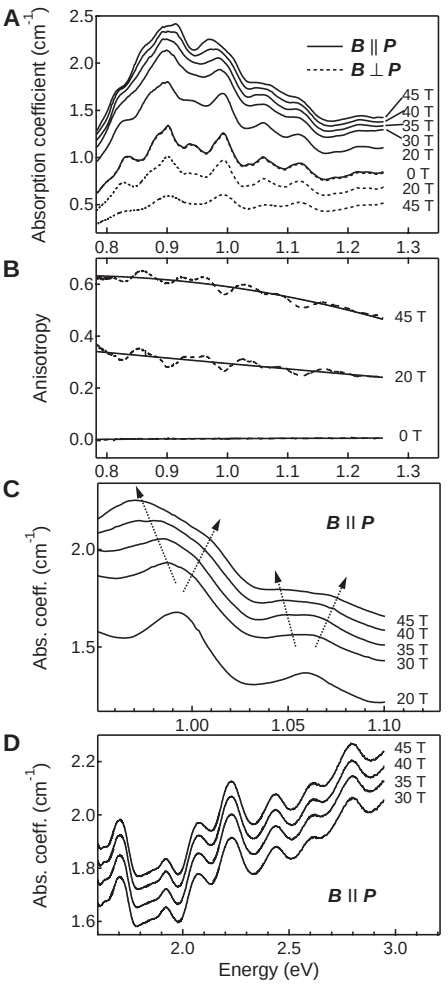

Fig. 2. (**A**) Polarization-dependent magneto-absorption spectra for sodium dodecyl sulfate (SDS)–suspended SWNTs in D_2O in the spectral range of the first-subband (E_1H_1) transitions. Solid and dashed lines are for parallel ($\boldsymbol{B}//\boldsymbol{P}$) and perpendicular ($\boldsymbol{B}\perp\boldsymbol{P}$) polarizations, respectively. No traces are offset. (**B**) Optical anisotropy, defined as $(\alpha_{//} - \alpha_{\perp})/(\alpha_{//} + \alpha_{\perp})$, versus photon energy. For a given field, the larger the nanotube diameter, the larger the optical anisotropy. (**C**) An expanded plot of data for the $\boldsymbol{B}//\boldsymbol{P}$ case from 20 to 45 T, showing the field-induced splitting of two absorption peaks. (**D**) Absorption spectra in the spectral range of the second-subband (E_2H_2) transitions at fields 30, 35, 40, and 45 T for $\boldsymbol{B}//\boldsymbol{P}$. No traces are offset. The linewidths are larger than in the E_1H_1 case, making splittings invisible, although optical anisotropy is clearly seen.

The chiralities (n,m) of the main five peaks, peaks 1 to 5, are indicated in the caption. It can be seen that all PL peaks exhibit interesting spectral evolution with B. Specifically, all peaks shift to lower energy, and the shift is more obvious for lower-energy peaks (peaks 1 and 2) or larger-diameter tubes.

Our observations can be explained in terms of the AB effect–induced AA splitting if we consider the magnetic alignment of nanotubes. The nanotubes align because of their highly anisotropic magnetic susceptibilities χ (*9*, *10*). When $\phi/\phi_0 \ll 1$, metallic tubes are predicted to be paramagnetic only along their axes ($\chi_{//} > 0$, $\chi_\perp < 0$, $|\chi_{//}| \gg |\chi_\perp|$), and semiconducting tubes are predicted to be diamagnetic in all directions ($\chi < 0$), but its negative χ is strongest perpendicular to their axes ($|\chi_{//}| < |\chi_\perp|$). This essentially dictates that a B would act on both metallic and semiconducting tubes with a torque that tends to align the tube along the B direction. This effect has been already used for making macroscopic films of aligned bundles of nanotubes (*18*).

Unlike Zeeman splitting, the amount of AA splitting depends on the angle between the tube and the field and can reach the maximum value when the tube is parallel to $\boldsymbol{B}$ because ϕ/ϕ_0 is then maximal. This explains why significant spectral changes were observed in absorption only for $\boldsymbol{P}$ parallel to $\boldsymbol{B}$. Unlike PL data, which show resolved peaks corresponding to different chiralities, an absorption peak can originate from several overlapping peaks corresponding to different chiralities present in the sample (*15*), which complicates the data analysis. Nevertheless, the fact that the splittings were observed for $\boldsymbol{B}//\boldsymbol{P}$, but not for $\boldsymbol{B}\perp\boldsymbol{P}$, demonstrates the angle-dependent nature of the observed AA splitting.

The 0-T PL data can be adequately fitted using Lorentzian peaks corresponding to specific chiralities (Fig. 3A). To take into account the angle distribution of nanotubes at finite fields, we use the Maxwell-Boltzmann statistics. The probability density that a given nanotube, consisting of N moles of carbon atoms, is at an angle θ relative to the field can be written as [see, for example, (*18*)]

$$\frac{dP(\theta)}{d\theta} = \frac{\exp(-u^2 \sin^2\theta)\sin\theta}{\int_0^{\pi/2} \exp(-u^2 \sin^2\theta)\sin\theta d\theta} \quad (1)$$

where $u \equiv \{B^2 N(\chi_{//} - \chi_\perp)/k_B T\}^{1/2}$ (k_B is the Boltzmann constant and T is temperature). The quantity u is a dimensionless measure of alignment, containing the ratio of the alignment energy to the thermal energy, and completely determines the angle distribution of an ensemble of nanotubes of the same length for a given chirality at given B and T. Starting from the 0-T fit, the angle-dependent splitting at 45 T, averaged over the angle distribution, was calculated by taking the 45-T AA splitting for a tube parallel to B and u as fitting parameters for each chirality present. The obtained 45-T fit is shown as a dashed curve in Fig. 3A, and the best values for u's and splittings are shown in Fig. 3, C and D, respectively. The obtained values for 45-T splitting are comparable to the predicted AA values; they are an order of magnitude larger than the 45-T Zeeman splitting (with $g = 2$). Larger u values are obtained for lower-energy (larger-diameter) peaks (Fig. 3D), which is consistent with absorption data (Fig. 2B) and is expected (*9*, *10*).

Our model implies that values for AA splitting and u's should be both proportional to the applied field B. As a critical test of these assumptions, calculations for intermediate fields were plotted using values for splittings and u's derived from the fitted 45-T values (Fig. 3B). Excellent agreement between the measured and calculated spectra further supports our model and conclusions. More specifically, the model reproduces the observed increase and decrease of PL peak widths with increasing B. This happens because of the fact that tubes having different angles with respect to B show different amounts of splitting (due to different values of ϕ). This inhomogeneous broadening disappears at small fields (because $\phi \sim 0$ for all tubes) and high fields (because the majority of tubes are then nearly parallel to the B direction).

These results not only verify the quantum theories based on the Bloch theorem and the AB phase but also open up possibilities for further studies of one-dimensional magneto-excitons in individually suspended and aligned SWNTs.

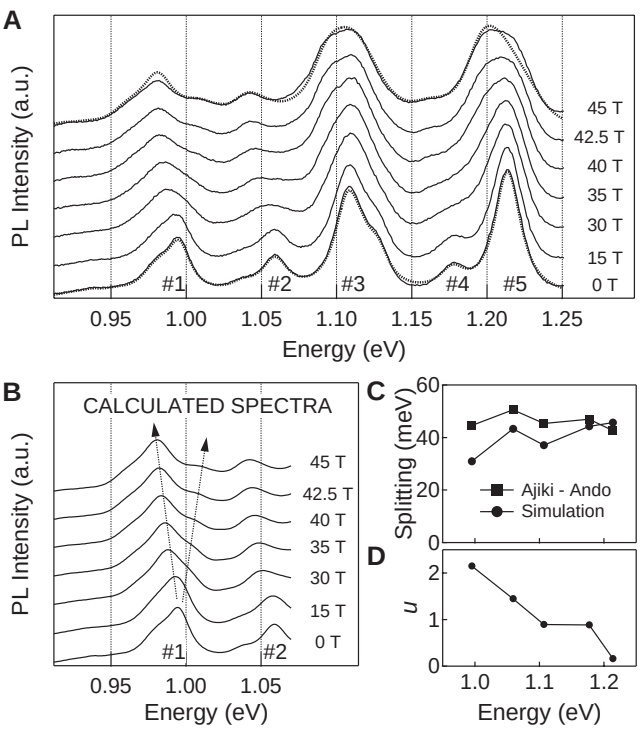

Fig. 3. (**A**) Magneto-PL spectra for SDS-suspended SWNTs in D_2O, excited with a 633-nm beam. The traces are shifted vertically for clarity. Solid lines correspond to measured data, and dotted lines correspond to fitted data. The chiralities of the most visible peaks are as follows: 1, (10,3); 2, (8,6); 3, (7,6); 4, (10,2); and 5, (7,5). As the field increases, all peaks redshift. (**B**) Calculated PL spectra at various fields for the first two peaks. The spectra are vertically offset for clarity. (**C**) AA splittings at 45 T obtained from predictions (*6*, *7*) (squares) and the simulation (circles). (**D**) The values of the alignment parameter u at 45 T for the five main PL peaks, obtained from our data analysis.

References and Notes

1. Y. Aharonov, D. Bohm, *Phys. Rev.* **115**, 485 (1959).
2. B. L. Altshuler, A. G. Aronov, B. Z. Spivak, *Pis'ma Zh. Eksp. Teor. Fiz.* **33**, 101 (1981) [*JETP Lett.* **33**, 94 (1981)].
3. A. G. Aronov, Yu. V. Sharvin, *Rev. Mod. Phys.* **59**, 755 (1987).
4. A. Bachtold *et al.*, *Nature* **397**, 673 (1999).
5. A. Lorke *et al.*, *Phys. Rev. Lett.* **84**, 2223 (2000).
6. H. Ajiki, T. Ando, *J. Phys. Soc. Jpn.* **62**, 1255 (1993).
7. H. Ajiki, T. Ando, *Phys. B* **201**, 349 (1994).
8. W. Tian, S. Datta, *Phys. Rev. B* **49**, 5097 (1994).
9. J. P. Lu, *Phys. Rev. Lett.* **74**, 1123 (1995).
10. H. Ajiki, T. Ando, *J. Phys. Soc. Jpn.* **62**, 2470 (1993).
11. P. J. Lin-Chung, A. K. Rajagopal, *Phys. Rev. B* **49**, 8454 (1994).
12. S. Roche *et al.*, *Phys. Rev. B* **62**, 16092 (2000).
13. F. L. Shyu *et al.*, *Phys. Rev. B* **67**, 045405 (2003).
14. M. J. O'Connell *et al.*, *Science* **297**, 593 (2002).
15. S. M. Bachilo *et al.*, *Science* **298**, 2361 (2002).
16. See supporting material on *Science* Online for details.
17. G. N. Ostojic *et al.*, *Phys. Rev. Lett.* **92**, 117402 (2004).
18. D. A. Walters *et al.*, *Chem. Phys. Lett.* **338**, 14 (2001).

19. Supported by the Robert A. Welch Foundation (through grant no. C-1509), the Texas Advanced Technology Program (through project no. 003604-0001-2001), and NSF (through grant no. DMR-0134058). A portion of this work was performed at the National High Magnetic Field Laboratory, which is supported by NSF cooperative agreement no. DMR-0084173 and by the State of Florida.

Supporting Online Material

www.sciencemag.org/cgi/content/full/304/5674/1129/DC1
SOM Text
Fig. S1
References

6 February 2004; accepted 14 April 2004